

DOI: <https://dx.doi.org/10.21123/bsj.2022.6508>

A Green Synthesis of Iron/Copper Nanoparticles as a Catalytic of Fenton-like Reactions for Removal of Orange G Dye

Ahmed K Hassan¹ 

Mohammed A Atiya² 

Imad M Luaibi² * 

¹Environment and Water Directorate, Ministry of Science and Technology, Baghdad, Iraq

²Al-Khwarizmi College of Engineering, University of Baghdad, Baghdad, Iraq,

*Corresponding author: emad.iq84@gmail.com

E-mail addresses: ahmedkhh71@yahoo.com , mohatiya1965@gmail.com

Received 12/8/2021, Accepted 20/9/2021, Published Online First 20/5/2022, Published 1/12/2022



This work is licensed under a [Creative Commons Attribution 4.0 International License](https://creativecommons.org/licenses/by/4.0/).

Abstract:

This research paper studies the use of an environmentally and not expensive method to degrade Orange G dye (OG) from the aqueous solution, where the extract of ficus leaves has been used to fabricate the green bimetallic iron/copper nanoparticles (G-Fe/Cu-NPs). The fabricated G-Fe/Cu-NPs were characterized utilizing scanning electron microscopy, BET, atomic force microscopy, energy dispersive spectroscopy, Fourier-transform infrared spectroscopy and zeta potential. The rounded and shaped as like spherical nanoparticles were found for G-Fe/Cu-NPs with the size ranged 32-59 nm and the surface area was 4.452 m²/g. Then the resultant nanoparticles were utilized as a Fenton-like oxidation catalyst. The degradation efficiency of OG dye highly depends on H₂O₂ concentration (1.7-5.28 mM), catalyst dose (0.4-1.6 g/L), pH (2-7), initial OG concentration (25-75 mg/L), and temperature (20-50 °C). Batch experiments showed that 94.8 % of 50 mg/L of OG dye was removed within the optimum peroxide concentration, dose, pH and temperature which were 3.52 mM, 1 g/L, 3, and 40°C respectively along with 30 min contact time. The results of kinetic models showed that OG removal followed the second-order model. Finally, the thermodynamic study of reaction was also examined and concluded to endothermic reaction with 29.725 kJ/mol activation energy.

Keywords: Fenton-like, Green synthesis, Iron/copper nanoparticles, Kinetics, Orange G dye.

Introduction:

Globally, dyes are produced up to thousands of tons yearly and used by many industries such as textile, leather, and printing. However, the release of these materials into effluent water impacts the ecosystem and causes pollution due to entering some risky elements in their production ¹. Further, dyes harm the esthetic of water, prevent absorption of sunlight, and photosynthesis ². Some literature confirmed that the azo structure contains benzene rings and the increase of these rings leads to rising toxicity ³. Orange G dye (OG) is one of the common synthetic azo dyes, it is easily dissolved in water and has been used to color textile products such as wool and silk. On the other hand, OG is a highly toxic anionic dye, the hazardous of this dye can be imputed to the azo group which is existing in its structure, furthermore, direct exposure to OG dye can impact the human digestive or respiratory ⁴. Therefore, various methods and technologies have

been used for treating dyes in wastewater. In the last few decades, the removal of dyes was accomplished using classical methods such as sedimentation and equalization ⁵. Recently, various technologies and techniques have been used for treating wastewater polluted with dyes including adsorption, chemical coagulation, ions exchange, membrane separation, photocatalysis and electrocoagulation ⁶, however, these technologies have their drawbacks represented by the formation of undesirable intermediates, expensive, and restricted in some applications ⁷. In the most recent decade, advanced oxidation technologies (AOTs) have emerged as potential alternative techniques to eliminate the organic contaminants derived from industrial effluents, these techniques provided a significant solution for removing the wastewater dyes and have the ability to treat the components that are resistant to traditional treatment technologies and without

generating secondary wastes⁸. The AOTs are performed by the activation of hydrogen peroxide (H_2O_2) and produced highly reactive and non-selective species like hydroxyl radicals ($\cdot\text{OH}$), these compounds have the capability to oxidize the organic pollutants existing at high concentrations⁹.¹⁰. Among the ATOs treatment methods, Fenton's-reagent has taken major attention due to the simplicity and eco-friendly of this method, it depends on the reaction between Fe^{2+} ions and H_2O_2 for producing very reactive compounds named hydroxyl radicals¹¹. However, there are some limitations with using Fe^{2+} ions related either by ferrous precipitation at the low pH or $\cdot\text{OH}$ scavenging for using a high concentration of H_2O_2 , thereby, the Fe^{2+} replaced by zero-valent iron (ZVI) nanoparticles which have proved a good catalyst to overcome the drawbacks. Therefore, the Fenton-like reactions are promising good techniques for the degradation of complex organic pollutants¹².

Different methods are used to synthesize ZVI such as the physical method that includes milling, vacuum sputtering, and thermal decomposition. Moreover, the chemical method uses borohydride (NaBH_4) as a reduction agent. These two methods may need a piece of sophisticated equipment, difficult conditions to control during the experiment, long procedures, and toxic capping agents. Therefore, the biological method is a promising technique to overcome these problems while achieving a safe and suitable procedure to synthesize nanoparticles, treatment technology from plant extract and microorganisms which have been used as an alternative to physical and chemical methods¹³. The biological synthesis using leaf extract of plants is shown to be a more promising technique due to economic feasibility and are not complex synthetic procedures. Plant leaves contain an extremely large amount of both capping and reducing agents like flavonoids, polyphenols, and other reducing components that have the ability to reduce the salts to zero-valent and prevent them from agglomeration. The abundance of plants that do not have chemicals with bad side effects, non-toxic, have high efficiency and are not expensive, have been approved to be used in synthesizing green nanoparticles which are going to be utilized in treating wastewater^{14, 15}. One of the most abundant evergreens in several Asian countries and the United States is the ficus tree. It belongs to the Moraceae family and can grow up to 30 meters in its normal habitat¹⁶. Ficus contains numerous bioactive compounds such as phenolic, flavonoids, alkaloids and tannins. These components are critical to the creation of ficus-zero valent iron nanoparticles (F- Fe^0) because they do not have negative or toxic side effects. They are also

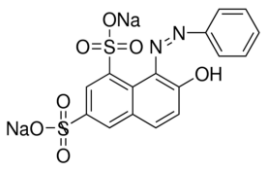
biodegradable, environmentally safe, and can act as capping and reducing agents¹⁷. Although iron nanoparticles (Fe-NPs) has become widely used as a promising metal in treatment processes for the removal of various environmental contaminants¹⁸, the reactivity of (Fe-NPs) may be impacted by the development of an oxide layer around particle surfaces¹⁹. To prevent this reaction, bimetal has been widely used to protect nanoparticles from oxidizing by adding a second catalyst such as Cu, Pt, Pd, Ni to Fe-NPs¹⁹. The mutual effect of two metals improves the properties of nanoparticles over the use of just one metal (monometallic); therefore, bimetallic nanoparticles have become of great interest to researchers^{20 21}. Due to the economically and safely uses of copper compared to Pd and Ni, it has been used for coating the catalyst to enhance the rate of decolourization¹⁹. The novel idea of removing OG by using a catalyst of bimetallic Fe/Cu nanoparticles synthesized by ficus leaves can be ascribed to the significance of using green chemistry methods that represent an alternative environmentally and not expensive ways, furthermore, the bimetallic catalyst of nanoparticles is more effective than mono-metal in the removal of various contaminants²².

In this study, green synthesis of iron/copper nanoparticles (G-Fe/Cu-NPs) was prepared using the extract of the ficus plant. Then the effects of experimental factors such as concentration of H_2O_2 , pH, the initial concentration of dye, temperature, and the dose of catalyst on the degradation of anionic Orange G dye using Fenton-like reactions have been investigated.

Materials and Methods: Chemical and reagents

The purity of all chemicals utilized was high (99.9 %), ficus leaves were collected from the University of Baghdad, Iraq. OG was purchased from Central Drug House (BDH) Company, and Table 1 shows the properties of this dye. Ferrous sulfate heptahydrate ($\text{FeSO}_4 \cdot 7\text{H}_2\text{O}$) was purchased from BDH company and copper sulfate pentahydrate ($\text{CuSO}_4 \cdot 5\text{H}_2\text{O}$) was purchased from Fluka AG company. The change of pH was adjusted using 1.0 M H_2SO_4 and 1.0 M NaOH solutions. The wavelength λ_{max} was specified using a UV/VIS spectrophotometer.

Table 1. Physicochemical characteristics of orange G dye (OG).

Properties of (OG) dye	
Molecular structure	
Molecular formula	C ₁₆ H ₁₀ N ₂ Na ₂ O ₇ S ₂
Molecular weight (g/mole)	452.37
Solubility in water	Soluble in water
Maximum wavelength (nm)	478

Catalyst Preparation

The G-Fe/Cu-NPs was prepared following the same procedures showed in the previous study²³, with some modifications as follows:

Step 1: Fresh ficus leaves were washed several times using tap water, and then washed with distilled water to eliminate any impurities or dust, followed by drying in an oven at 60 °C. Additionally, they were cut using mortar and pestle into small pieces with sifting using a 2.5mm sieve.

Step 2: The ficus leaf extract is prepared in 150 ml of deionized water with 20 g of ficus leaf pieces which were then boiled at 70°C for 20 min and then filtered using filter paper to remove suspended ficus particles. Finally, the filtrate is refrigerated at 4°C until used as a reducing and capping agent.

Step 3: A solution of 1.494 g of FeSO₄.7H₂O and 0.7g of CuSO₄.5H₂O salts were dissolved in 100 ml of deionized water. After the salts had completely dissolved, the filtration process using a filter paper was followed to remove any impurities. To develop the synthesis of G-Fe/Cu-NPs, 100 ml of extract from step 2 was added dropwise to the 100 ml of Fe (II) / Cu (II) mixture. After several drops of ficus extract were added, the mixture's color changed gradually from yellow, brown, and finally to black indicating the metals equivalent were reduced to zero-valent and the formation of G-Fe/Cu-NPs completed. The remaining ficus extract is added to accelerate the reduction. In addition, the mixture is stirred continuously at 300 rpm by using a magnetic stirrer for 15 min. The black precipitate of G-Fe/Cu-NPs nanoparticles was separated by vacuum filtration using filter paper and immediately washing process was involved using distilled water three times, followed by rinsing with absolute ethanol. The washing and rinsing processes are important steps in the synthesis because they prevent the fast oxidation of nanoparticles. The G-Fe/Cu-NPs were then dried overnight at ambient temperature and then ground by mortar and pestle to a fine powder. Fig. 1 illustrates the green synthesis of G-Fe/Cu-NPs.

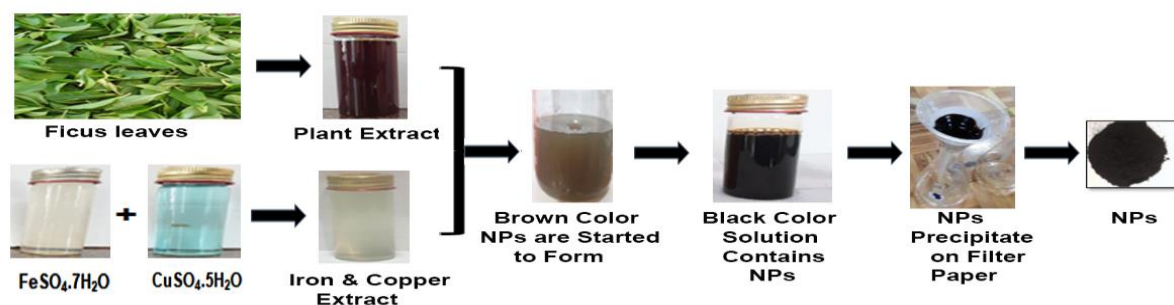


Figure 1. Schematic illustration of G-Fe/Cu-NPs synthesis.

Analytical Methods

Before starting the experiments, a calibration curve for standard OG solution was done to locate the maximum wavelength (λ_{max}) of dye and the equation that joined the absorbance with concentration. Thus, the λ_{max} of OG was found to be 478 nm as shown in Fig.2.

According to the below formula the removal efficiency (RE) was calculated:

$$RE \% = \frac{C_o - C_t}{C_o} \times 100 \quad \dots 1$$

Where the C_o is the initial concentrations and C_t is the OG concentration at time t.

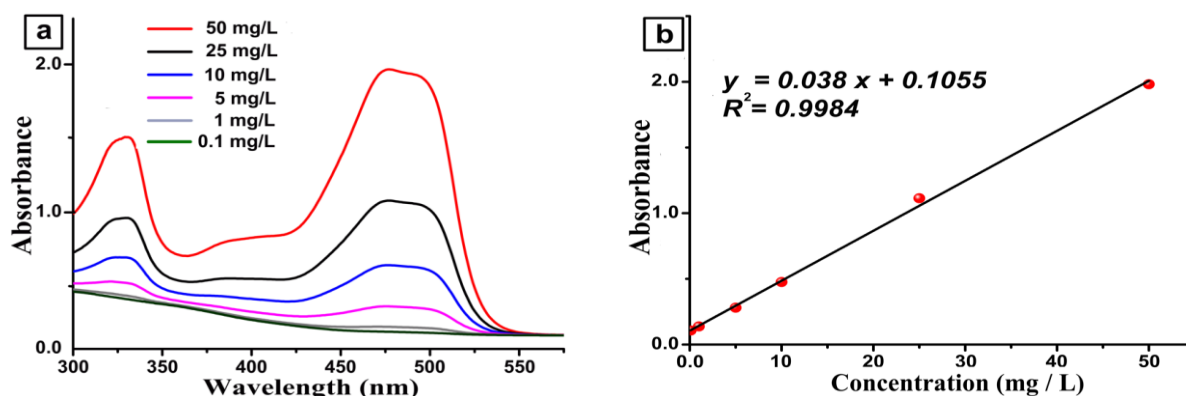


Figure 2. UV-Vis analysis for various concentrations of OG solutions (a) Absorption and (b) Calibration curve.

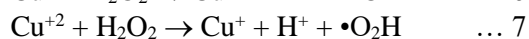
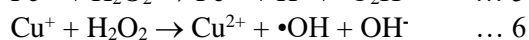
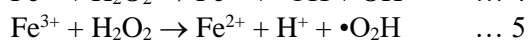
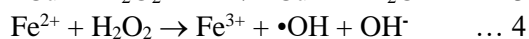
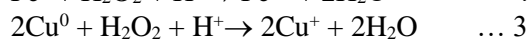
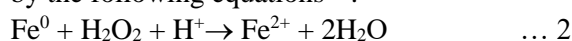
Batch Fenton-like Experiments

In Fenton-like processes, the experiments would be carried out to evaluate the OG removal efficiency. A working solution of 50 mg/L of OG was prepared by dissolving 0.05 g of dye in 1L deionized water, followed by adjusting pH by using 1.0 (by 1.0 M H_2SO_4 and 1.0 M NaOH) before adding G-Fe/Cu-NPs and H_2O_2 . Some operating parameters were changed including hydrogen peroxide concentrations ranged (1.7- 5.28 mmol/L), G-Fe/Cu-NPs dosage ranged (0.4–1.6 g/L), pH ranging from (2-7), the range of initial OG concentrations were (25–75 mg/L), contact time interval up to 120 min, the temperature ranged from (20-50 °C), and coexisting NaCl from (0.5 – 50 g). A particular amount of G-Fe/Cu-NPs was supplemented to the OG solution followed by mixing for 1 minute to homogenize the catalyst, after that, the H_2O_2 at a certain concentration was added and agitated at 300 rpm using a magnetic hot plate. The parameters were optimized separately by maintaining all operating conditions constant except for the one that wants to optimize. During each run, 10 ml samples were taken at a regular time and mixed with prepared 200 μ l of 1M Na_2SO_3 in the vial, then they were analyzed by UV/VIS spectrophotometer after filtering them using 0.22 μ m membrane filter. The purpose of adding Na_2SO_3 is just to quench the reaction⁸. The removal efficiency was measured using Eq. 1.

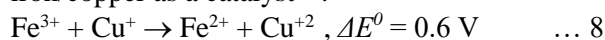
Mechanism of Reaction

The possible mechanism of the reaction between iron/copper nanoparticles and hydrogen peroxide can be expressed by approaching the hydrogen peroxide to the nanoparticle and reacts with these particles, followed by oxidizing the zero-valent iron/copper to form Fe^{+2} and Cu^+ where the electrons of iron and copper nanoparticles transferred from NPs to H_2O_2 , as a result, the iron/copper ions are activated by hydrogen

peroxide, thereby, to generating $\bullet OH$ as illustrated by the following equations²⁴:



In the electrochemical regard, the presence of copper ions contributes to reducing Fe^{+3} to Fe^{+2} (Eq. 8) due to variance in potential between Fe^{+3}/Fe^{+2} (0.77V) and Cu^{+2}/Cu^+ (0.17V). This reaction is very important in improving the decomposition of H_2O_2 and accelerates the pollutants degradation process. Therefore, the $\bullet OH$ formation and the oxidative process kinetics are highly developed in the presence of bimetallic iron/copper as a catalyst²⁴.



Results and Discussion:

Characterization of G-Fe/Cu-NPs

Some techniques are utilized to prove the chemical classification, structure, size, and surface area of nanoparticles. The morphology, topography, and average size of these nanoparticles were characterized by a scanning electron microscopy (SEM) model. The EDAX technique is a confirmatory method used to ensure the identification and chemical classification of each particle, the EDAX detector and SEM model was (TESCAN MIRA 3, Czech Republic). In addition, AFM characterization is very helpful for determining the morphology of nanoparticle surfaces, it measures the contact force between the tip and surface, the model of AFM test which was tested on the G-Fe/Cu-NPs is (TT-2, USA). Furthermore, the XRD system is also utilized to investigate the crystallinity of the materials. The major picks using the XRD system can accurately

determine the crystalline nature of nanoparticles, the XRD test was already applied on the nanoparticles using (Philips X'pert diffractometer) model. In addition, FT-IR spectroscopy is widely used to confirm the structure of unidentified compounds, as well as to determine the functional group of numerous materials, especially for biomaterials, and (Shimadzu, Japan) was the FT-IR spectroscopy model in this work. The BET technique determines the specific surface area, the size radius of average pore, average porosity radius, and pore volume of nanoparticles, the G-Fe/Cu-NPs subjected to the BET test by the device model (TriStar II Plus Version 2.03, USA). At last, zeta potential is widely used to inspect the potential stability of the colloid nanoparticles. The high positive or negative zeta potential for colloids tends to be stable electrically while low zeta potential for colloids is flocculated or coagulated.

As a result, the variances in the color of the solution from yellow, brown, and then to black indicate the reduction process happened and formation of G-Fe/Cu-NPs, as well as the variation in the pH before and after the reduction process, where the pH of the ficus extract was 5.42 and the pH of the mixture after reduction was 3.24. As a

result, along the reduction route, the pH of the solution declines and goes to the higher acidic range.

The scanning electron microscopy (SEM) images showed that the synthesized G-Fe/Cu-NPs were porous and shaped like spherical with diameters ranging from 32-59 nm (Fig. 3a and Fig.3b). Additionally, the porous and hollows in the nanoparticles improve dye removal. Moreover, the size variation of NPs created was due to the variation of the local concentration of the ficus extract which was responsible to reduce the metal ions.

The Energy Dispersive Spectroscopy (EDAX) of nanoparticles presented in Fig. 4b contains further information about the synthesis of G-Fe/Cu-NPs, where the place of atomic distribution and chemical composition of the catalyst was demonstrated by the intense peaks of Fe, Cu, C, and O, 5.51 wt%, 3.33 wt%, 48.67 wt%, and 42.49 wt%, respectively. The finding of adjoint elements such as C and O signals resulted mainly from the ficus extracts that contain organic compounds such as C and O molecules which play a major role in the reduction and stabilizing process of G-Fe/Cu-NPs^{25, 15}.

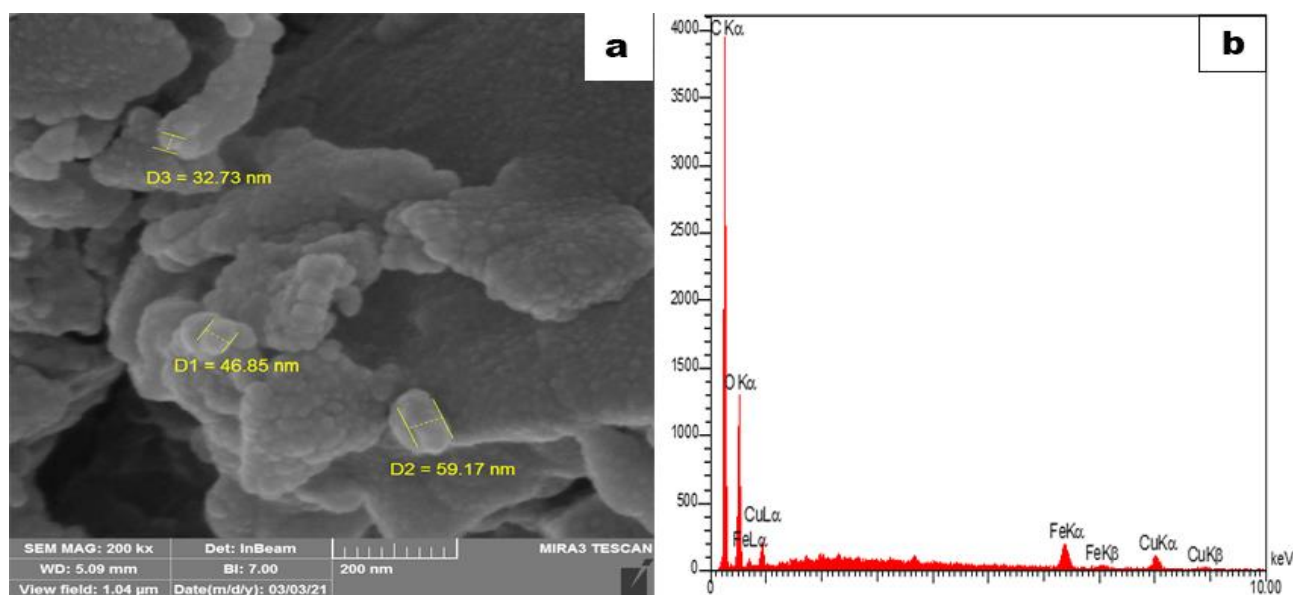


Figure 3. (a) SEM images of G-Fe/Cu-NPs, (b) EDAX of the prepared G-Fe/Cu-NPs sample.

According to the atomic force microscopy (AFM) images of G-Fe/Cu-NPs, the high rough surface through hills and valleys shape with a nano-rough texture and homogenous of nanoparticles can be seen in Fig. 4 which indicates the amorphous and

granular shape of G-Fe/Cu-NPs. This roughness enhances the capability of the surface of the nanoparticles to adsorb dye ions. Furthermore, the average size distribution of G-Fe/Cu-NPs tested by AFM ranged between (7.5-23 nm).

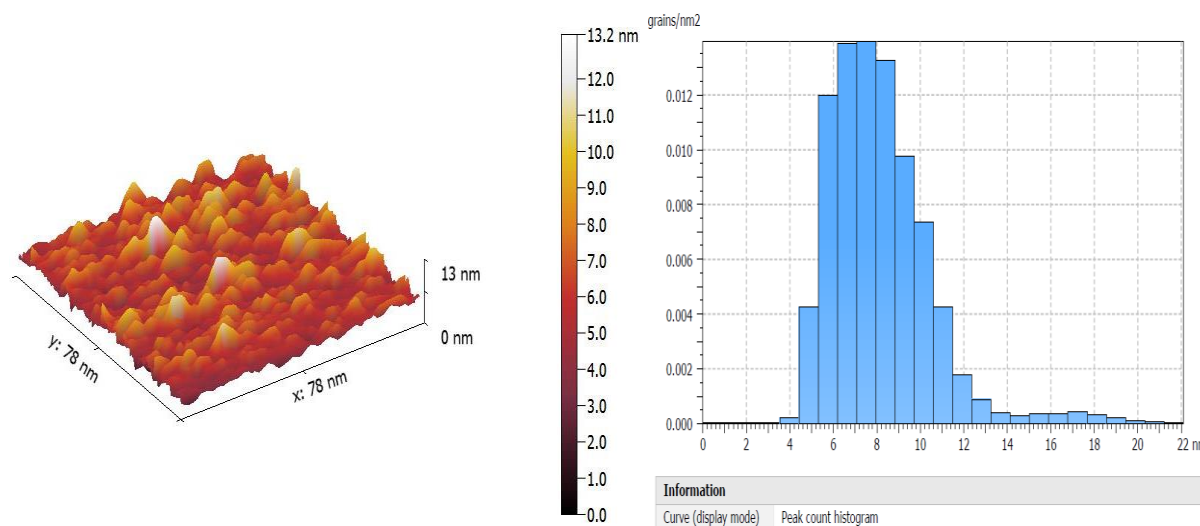


Figure 4. Atomic force microscopy (AFM) characterization for G-Fe/Cu-NPs.

The FT-IR for preparing G-Fe/Cu-NPs is taken in the band range $400\text{-}4000\text{ cm}^{-1}$ to ensure the functional group of these nanoparticles as depicted in Fig. 5, the O-H stretching vibrations illustrated in the band between $3220\text{-}3430\text{ cm}^{-1}$ belong to polyphenol compounds which play an important role in reducing the Fe/Cu metals and then synthesis

of bimetallic nanoparticles¹⁵. The amide group in the prepared nanoparticles can be noticed at band 1614 cm^{-1} which indicate the presence of flavonoids, polyphenols and proteins in ficus leaf, these compounds attribute to reduce the formation of G-Fe/Cu-NPs¹⁶.

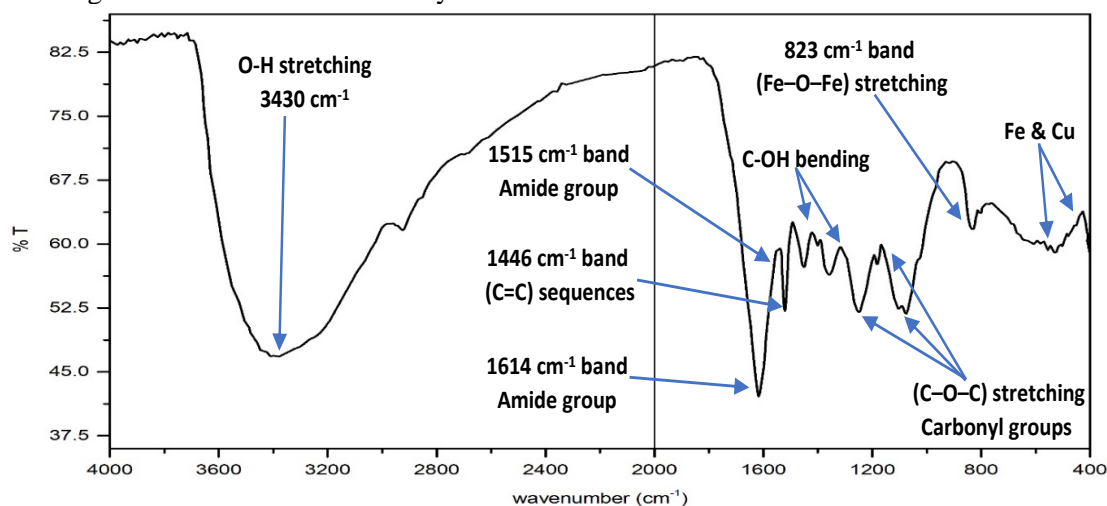


Figure 5. FTIR spectrum of prepared G-Fe/Cu-NPs samples.

The C=C sequences at 1446 cm^{-1} are attributed to the aromatic ring, while the bands at 1396 and 1244 cm^{-1} is related to C-OH bending, respectively²⁶. The band observed at 823 cm^{-1} is related to the (Fe-O-Fe) stretching, and the vibration broadband ranged between $549\text{-}403\text{ cm}^{-1}$ could be assigned as Fe/Cu nanoparticles²⁷. The peaks ranged from 1174 to 1070 cm^{-1} are caused by the carbonyl groups (C-O-C) stretching, these groups have the capability to prevent nanoparticles agglomeration by producing capping agents²⁸. The phenolic compounds of ficus leaf extract adsorbed on the prepared nanoparticles are confirmed by the mentioned peaks. Furthermore, these phenolic

compounds provide more stability to the nanoparticles when they were adsorbed on the surface of particles and act as a capping agent²⁹. As a result, the FT-IR analysis proved the ability of the ficus leaf for doing the stabilizing and reducing functions for G-Fe/Cu-NPs.

The XRD curve of synthesized nanoparticles is revealed in Fig. 6 which is not including any sharp peaks indicating there is no crystal structure in this case, even with a wide range of diffraction peaks (from $20^{\circ}\text{-}25^{\circ}$). The above result proves that the bimetallic G-Fe/Cu-NPs prepared by the green method are amorphous³⁰. The XRD result is in agreement with what had been concluded by^{31, 30}.

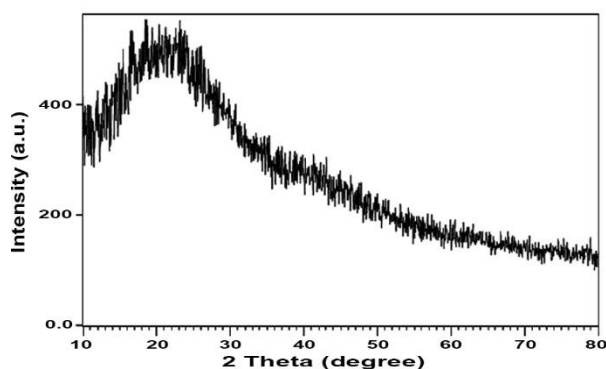


Figure 6. X-Ray diffraction (XRD) of G-Fe/Cu-NPs sample.

Table 2 shows the results of G-Fe/Cu-NPs surface area obtained by the BET technique. In this analysis, the pore size for G-Fe/Cu-NPs was 40.4 nm which can be classified as mesopore according to the classification of the IUPAC that categorized the pore size as macropore (>50 nm), mesopore (2 to 50 nm), super-micropore (0.7 to 2 nm) and ultra-micropore (<0.7 nm). Thus, as the catalytic performance is highly dependent on accessible pore channels due to their benefits for the diffusion of material, these sizes of pores provide more stability by acting as a shielding agent to prevent the harsh reaction conditions of the nanoparticles' active sites²⁷.

Table 2. BET parameters for G-Fe/Cu-NPs

Parameter	Value
BET (m ² /g)	4.452
Pore size (nm)	40.4
Pore volume (cm ³ /g)	0.0108

The high values of zeta potential provide the stability to nanoparticles for resisting the aggregation, while the small potential leads to flocculate. As shown in Fig. 7, a high negative value at (-51.47 mV) was obtained from zeta analysis provides good stability of G-Fe/Cu-NPs, this stability derives from existing phenolic compounds in the ficus leaf extract¹⁷.

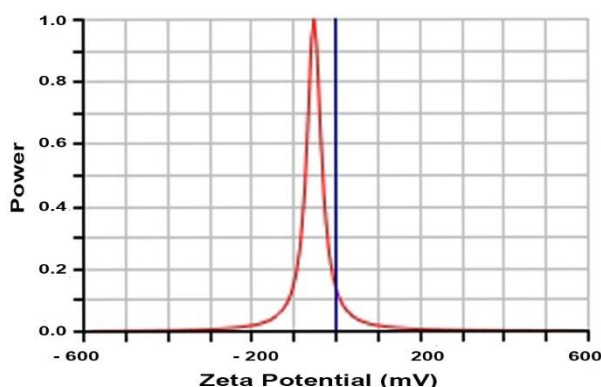


Figure 7. Zeta potential analysis for sample of G-Fe/Cu-NPs.

Effect of Parameters on the Degradation efficiency of OG dye

Effect of H₂O₂ Concentration

The existence of proper amounts of H₂O₂ in a satisfied concentration is a crucial matter in the Fenton-like reactions for generating the highly active $\cdot\text{OH}$ radicals³², therefore, the influence of H₂O₂ concentrations was investigated. Initially, one experiment was carried out by adding a certain amount of H₂O₂ without adding any amounts of the catalyst to examine if any reaction may be observed between OG solution with H₂O₂, and the result showed not. The concentration of H₂O₂ was changed in the range 1.7-5.28 mmol/L by keeping the rest of the experimental factors constant (G-Fe/Cu-NPs dosage 0.4 g/L, pH 4, initial OG concentration 50 mg/L, temperature 30°C, and agitation speed 300rpm). The results showed that the removal rates of OG were 30.9, 47.1, 72.8, 65.9, and 56.6 % for concentrations 1.7, 2.64, 3.52, 4.4, and 5.28 mmol/L respectively, at 120 min period time. As illustrated in Fig. 8, the efficiency increased with increasing H₂O₂ from 1.7 to 3.52 mmol/L and this was attributed to more production of very reactive $\cdot\text{OH}$ radicals.

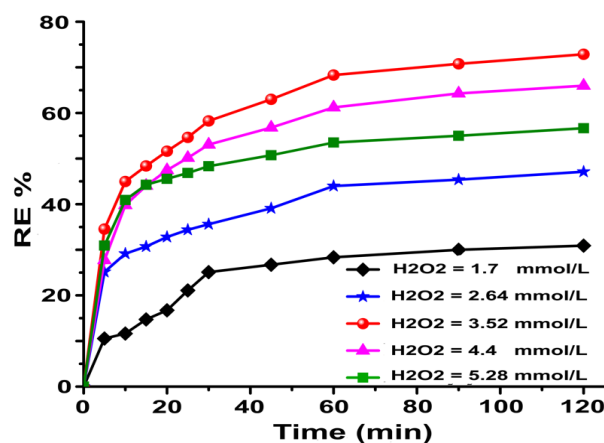
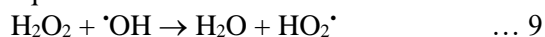


Figure 8. Effect of H₂O₂ concentration at the dose of G-Fe/Cu-NPs, initial OG concentration, pH, temperature, and agitation rate were 0.4g/L, 50 mg/L, 4, 30°C, and 300 rpm.

Nevertheless, it can be noticed that with the continuous rising of H₂O₂ concentration (as in 4.4 and 5.28 mmol/L) the removal efficiency decreased. The diminish of efficiency, in this case, can be explained by recombination of $\cdot\text{OH}$ with H₂O₂ that led to gradually reducing the number of $\cdot\text{OH}$ radicals in the solution and replaced with less reactive HO₂ \cdot ⁷ as illustrated in the following equation:



In general, the removal efficiency of OG increases with increasing as the hydrogen peroxide

concentration till reaching critical concentration and then the removal drops down. However, the excess of H_2O_2 of more than critical concentration would lead to a phenomenon known as a scavenging effect where the removal of dye decreases. Therefore, the H_2O_2 amount of 3.52 mmol/L was selected as the optimum concentration for subsequent experiments. This result was in agreement with a previous conclusion of removal Acid Black 1 reported by ³³.

Effect of Catalyst Doses

The catalytic activity of the G-Fe/Cu-NPs prepared by ficus leaves extract was also studied. Therefore, a set of experiments was carried out by changing the dosage of nanoparticles in the range 0.4-1.6 g/L with maintaining the rest of operating conditions as H_2O_2 concentration, pH, initial OG concentration, temperature, and agitation speed at 3.52 mmol/L, 4, 50 mg/L, 30°C, and 300 rpm respectively. Accordingly, the removal rates of OG were 86.5, 87.6, 91.6, 83.7, and 69.3 % for doses 0.4, 0.7, 1.0, 1.3, and 1.6 g/L respectively, at 120 min period time. Fig. 9 clearly shows that the removal efficiency of OG increased with the rising amount of G-Fe/Cu-NPs up to a certain dose, thereby the performance decreased with a higher catalyst amount indicating the uselessness of adding more quantities than the critical limit. The reason was related to the presence of ficus polyphenols compounds surrounded the catalyst surface, these compounds may be discharged to a working solution and reacted with $\cdot OH$ radicals ⁸. On the other hand, the low amount of G-Fe/Cu-NPs led to a decrease in the removal performance of OG due to the low $\cdot OH$ radicals' concentration at this catalyst dose ³⁴. Hence, the optimum catalyst dosage for the current study was 1 g/L. Similar behaviour in the removal of malachite green was found by ³⁵.

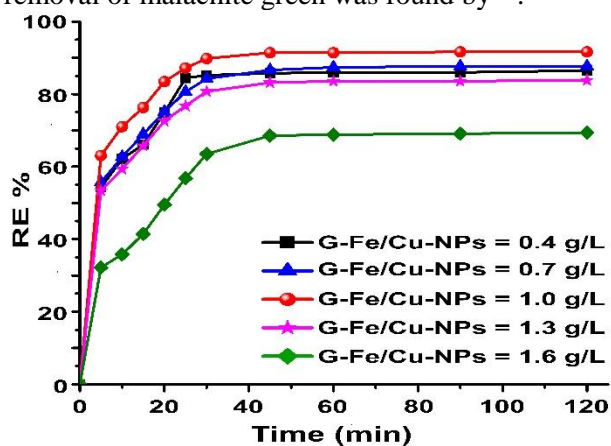


Figure 9. Effect of G-Fe/Cu-NPs dosage at H_2O_2 concentration, initial OG concentration, pH, temperature, and agitation rate were 3.52 mmol/L, 50 mg/L, 4, 30°C, and 300 rpm.

Effect of pH

In the Fenton-like process, the removal of organic pollutants is highly influenced by pH value, due to its impact on the catalyst performance, stability of H_2O_2 , and the generation of very reactive $\cdot OH$ radicals. Fig. 10 demonstrates the OG removal efficiency at various pH 2, 3, 4, 5, and 7 along with 120 min, whereas the other experimental factors were kept constant. The OG removal efficiencies were 76.1, 92.5, 91.6, 17.3, and 9.3 % respectively. The results revealed that the removal efficiency of OG was decreased with raising the pH of the solution, and the best removal performance of OG was at pH 3. The explanation of this behavior belongs to the Fenton-like mechanism and production of $\cdot OH$, where the reaction between Fe^0 with H_2O_2 is enhanced at the low pH values through the ions exchange to generating Fe^{+2} as the ions surrounded the surface of catalyst that in turn react with H_2O_2 and producing free radicals $\cdot OH$. In addition, the high acidic medium at the pH below 3 led to provide excessive amounts of H^+ ions which, in turn, contributed to reducing the number of very reactive $\cdot OH$ and therefore decreasing the degradation efficiency ³⁶. The reduction of $\cdot OH$ leads to the inability of converting Fe^{+3} to Fe^{+2} efficiently ³⁷. Furthermore, the ferrous ions and hydrogen peroxide are unstable at higher pH values (above 4), therefore, the catalyst would be precipitated and generate complex byproducts (ferric hydroxo complexes) which thereby leads to decomposition of the H_2O_2 and lowering the removal efficiency ³⁸. Notably, the removal of OG dye at these higher pH values was conducted by coagulation or sorption, not the oxidation process ³⁹. Several studies have reported the same conclusion such as ⁴⁰ and ⁴¹.

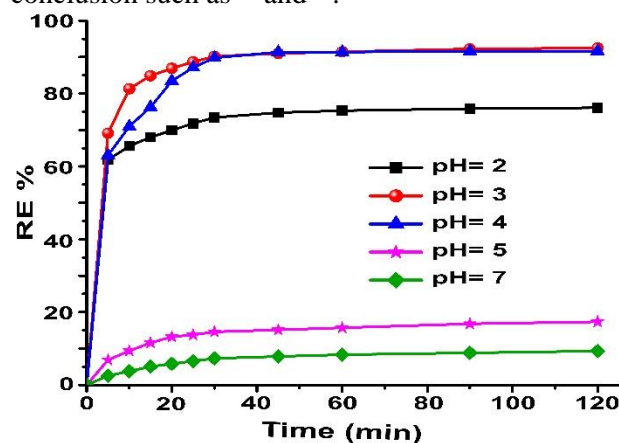


Figure 10. Effect of pH at G-Fe/Cu-NPs dosage, H_2O_2 concentration, initial concentration, temperature, and agitation rate were 1.0 g/L, 3.52 mmol/L, 50 mg/L, 30°C, and 300 rpm.

Effect of Initial OG Concentration

Generally, the degradation rate is a function of the initial concentration of dye, which make it a crucial parameter to be considered for effective Fenton-like. Thus, several OG concentrations of 25, 35, 50, 65, and 75 mg/L were used to investigate the impact of these concentrations on degradation efficiency. The other experimental factors were fixed (G-Fe/Cu-NPs=1.0 g/L, pH=3.0, temperature=30 °C, agitation speed=300 rpm) and removal rates were 97%, 93.8%, 92.5%, 85%, and 76.3% respectively. Therefore, it is concluded along the 30 min of reactions that the removal efficiency of OG decreased from 94.4% to 75.5 as the increase of dye concentration from 25 to 75 mg/L thereby led to lowering the concentration of radicals Fig. 11. As a result, the degradation of OG diminishes with increases in the dye concentrations, which indicated that the production and scavengers of high reactive $\cdot\text{OH}$ could be affected by the higher dye concentration, where the $\cdot\text{OH}$ radicals scavenging effects occur slightly when the dye concentration rising without exceeding the optimum $\cdot\text{OH}$ radicals value⁴¹. Therefore, this study selected 50 mg/L as the optimum initial concentration. Similar results were reported by¹¹.

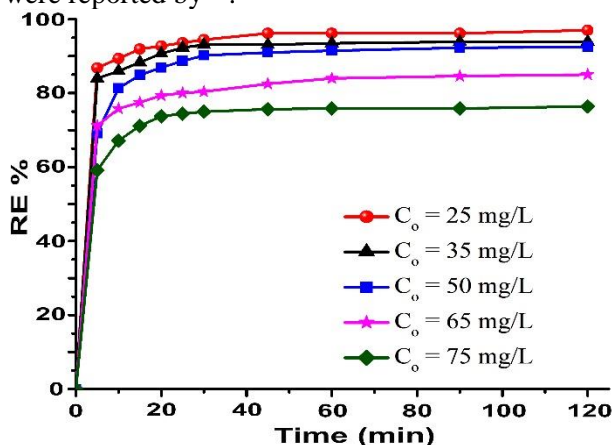


Figure 11. Effect of initial OG concentration at G-Fe/Cu-NPs dosage, H_2O_2 concentration, pH, temperature, and agitation rate were 1.0 g/L, 3.52 mmol/L, 3, 30°C, and 300 rpm.

Effect of Inorganic Salts

As a matter of fact, the real wastewater commonly contains amounts of inorganic salts such as NaCl which may impact the performance of dye degradation through the heterogeneous Fenton process. Therefore, various concentrations of NaCl were used to investigate the influence of the presence of these salts on OG dye degradation. Based on this purpose, 0.5, 10, and 50 g/L were introduced with maintaining the experimental conditions constant (G-Fe/Cu-NPs=1.0 g/L, H_2O_2 =3.52 mmol/L, pH=3, initial concentration=50 mg/L,

temperature=30°C). As shown in Fig. 12, the removal of OG efficiencies for the above NaCl concentration were 90%, 85.5%, and 77.5% respectively. It should be noted that the removal efficiency under the same conditions and without the presence of NaCl was 92.5%.

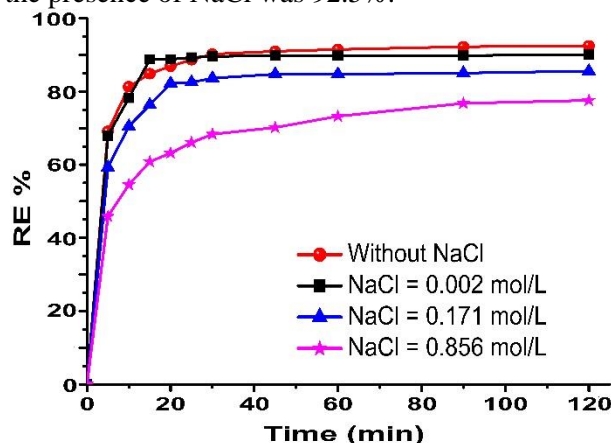
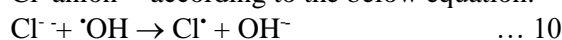


Figure 12. Effect of presence NaCl on the removal OG at catalyst dose, H_2O_2 concentration, initial OG concentration, pH, temperature, and agitation rate were 1.0 g/L, 3.52 mmol/L, 50 mg/L, 3, 30°C, and 300 rpm.

It was obvious that the presence of Cl^- anion had a negative impact on the OG removal performance, and this effect is directly proportional to increasing the concentrations of these compounds. The decrease in the rate performance was attributed to the accumulation of Cl^- anion on the G-Fe/Cu-NPs surface which led to blocking the active sites on this surface, another reason may belong to OH radicals scavenging by the effect of Cl^- anion⁴² according to the below equation:



The same behaviour of removal of sulfanilic acid azochromotrop dye by the Fenton process was reported by⁴³.

Effect of Temperature

Temperature plays an important role in dye degradation via a Fenton-like process. Therefore, further experiments were carried out to examine various temperature effects on the OG degradation by heterogeneous Fenton-like reaction. For this purpose, different temperatures (20, 30, 40, and 50 °C) were used with maintaining the other experimental conditions fixed (H_2O_2 = 3.52 mmol/L, catalyst dose =1.0 g/L, pH =3, initial OG concentration=50 mg/L, agitation speed =300 rpm). The results revealed that the removal efficiencies for the studied temperature were 87.2%, 92.5%, 95.3%, and 90.3% respectively at the end of 120 min as shown in Fig. 13. It can be notified that the raising in temperature led initially to improving the removal performance, moreover, the removal

efficiency of dye increased during the first 10 min from 72.7 to 92.1 % for the temperature range of 20 to 50 °C. Therefore, the increase of removal performance was attributed to an increase in the rate of production of high reactive $\cdot\text{OH}$ radicals⁴⁴, where rising in the temperature could be led to motivate hydrogen peroxide and react efficiently with G-Fe/Cu-NPs which thereby growing the rate product of hydroxyl radicals⁴⁵. Besides, the rate of $\cdot\text{OH}$ radical and OG dye interactions was enhanced by the increasing temperature resulting in rapid degradation³⁵. Anyway, it was evident that the rate of color removal at the end of 120 min diminished from 92.1 to 90.3% by the cause of decomposition of hydrogen peroxide at 50 °C reaction temperature⁸. These results agree with research papers published for the Fenton-like degradation of methylene blue⁴⁶.

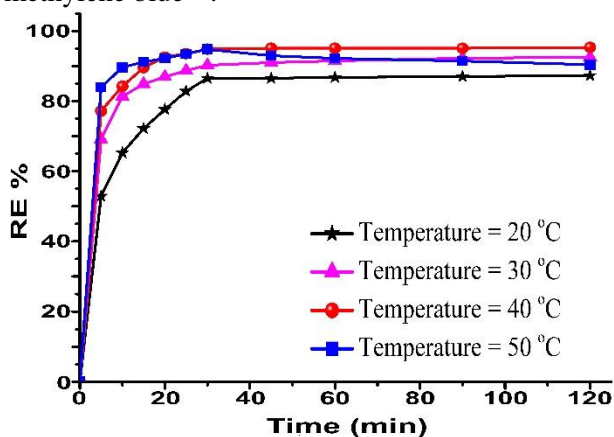


Figure 13. Effect of temperature on the removal OG at G-Fe/Cu-NPs dosage, H₂O₂ concentration, initial OG concentration, pH, and agitation rate were 1.0 g/L, 3.52 mmol/L, 50 mg/L, 3, and 300 rpm.

Kinetic of degradation OG by Fenton-like reactions

The kinetic models are used to analyze the degradation rate of pollutants. The mechanism of $\cdot\text{OH}$ radical-mediated is the major function of the Fenton process for degradation of dye, where the reaction between catalyst and hydrogen peroxide can produce $\cdot\text{OH}$ radicals which thereby attack the compounds of dye⁴⁷. Hence, Fenton-like kinetics models were engaged to estimate the decolorization data, including the zero-order, first-order, and

second-order⁴¹. Moreover, the Fenton-like process includes many-step reactions which made it a complex process⁴⁸. Therefore, the removal kinetics of OG by the Fenton-like was investigated at the varying period time 0-30 min with experimental conditions such as concentration in the range of (25-75 mg/L), H₂O₂ concentration of (1.7-5.28 mmol/L), a dosage of nanoparticles (0.4 - 1.6 g/L), initial pH (2 - 7), temperature (20 - 50°C), and co-existing NaCl (0.5 - 50 g/L) respectively for each factor. In order to investigate the above kinetics, Table 3 shows the kinetic equations were used:

Table 3. Kinetic equations

Model	Equation	Parameters
Zero-order	$C_t = C_o - k_0 t$	k_0 : zero-order rate constant (M. min ⁻¹). t : time (min)
First-order	$\ln C_t = \ln C_o - k_1 t$	k_1 : first-order rate constant (min ⁻¹)
Second-order	$\frac{1}{C_t} - \frac{1}{C_o} = k_2 t$	k_2 : second-order rate constant (g/mg.min)

The value of k_0 can be calculated from the slope of C_t against t , the values of these parameters with the regression coefficient were inserted in Table 4. Obviously, the values regression coefficient R^2 for all studied parameters of this model were not high enough indicating that they are poorly fitted with the zero-order model. On the other hand, the value of k_1 can be obtained from the slope of the natural logarithm of C_t versus t . As illustrated in Table 4 that the first-order was not fitted of degradation OG by the Fenton-like process due to had low values of R^2 . For the second-order kinetic model, the value of k_2 can be calculated from the slope of $1/C_t$ versus t graph. It can be seen from Table 4 that the linear fitting value of the regression coefficient R^2 for the second order is higher than those for zero-order and first-order, which indicates that second-order kinetic model is a fitted model for OG kinetic degradation by the Fenton-like process catalyzed by G-Fe/Cu-NPs. Further, Fig. 14 shows the second-order kinetics for all studied parameters.

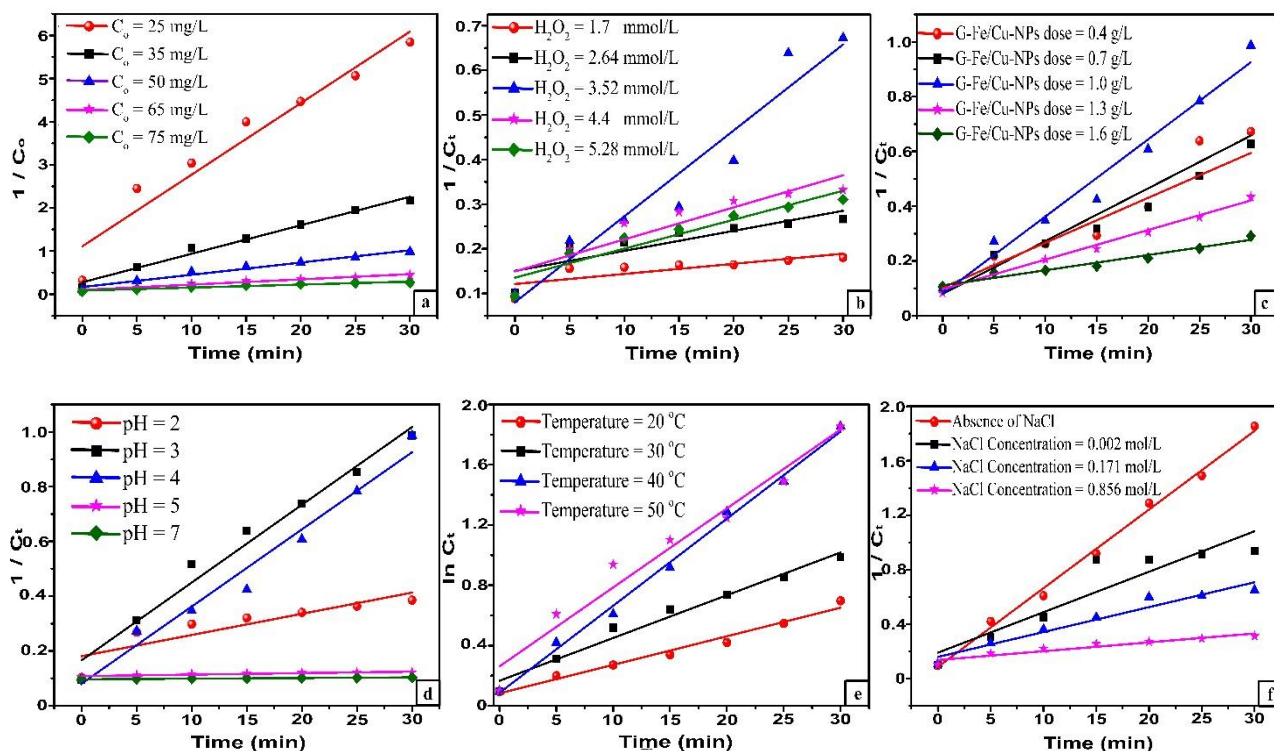


Figure 14. Second-order kinetic model for (a) initial OG concentration, (b) H_2O_2 concentration, (c) G-Fe/Cu-NPs doses, (d) pH, (e) temperature, and (f) co-existing inorganic salts.

Moreover, Table 4 shows that the increase of initial OG concentration from (25 to 75 mg/L) led to a decrease in the rate constant (0.166 to $0.007 M^{-1}.min^{-1}$) attributed to lowering the hydroxyl radicals. Besides, when the amount of H_2O_2 was raised of (1.7 to 3.52 mmol/L) the removal of OG increased and that ascribed to increase the $\bullet OH$. In contrast, the excess amount of peroxide (from 3.52 to 5.28 mmol/L) led to a decrease in the rate constant for the reason of $\bullet OH$ scavenging. Additionally, the high amount of catalyst resulted in an increase in the degradation rate due to increasing the concentration of $\bullet OH$. Otherwise, high G-Fe/Cu-NPs concentrations resulted in a decrease in the degradation rate, this was attributed to scavenging the $\bullet OH$ by the high amount of Fe^{+2} ⁴⁴. Furthermore, the k_2 increased with increasing the

temperature due to enhancing the reaction between G-Fe/Cu-NPs and H_2O_2 at the higher temperature thereby more formation of $\bullet OH$. Otherwise, because of the thermal decomposition of H_2O_2 , the rate of degradation was decreased at a temperature higher than 313K.

In conclusion, the kinetic behaviors of degradation OG followed two stages, the first one was fast degradation due to the reaction between hydrogen peroxide and ferrous ions, while the second stage is the slow progress of decolorization which can be attributed to accumulation of ferrous ions and decline their activity⁴⁹. Furthermore, Table 4 demonstrates that the second-order kinetic was the best fitted for OG degradation as evident from the higher values of correlation coefficient (R^2). The same results had been concluded by⁵⁰.

Table 4. The kinetics parameters for the Fenton-like reactions of the degradation OG.

Parameter		RE% after 30 min	RE% after 120min	Zero-order		First-order		Second-order	
				k_o (M.min ⁻¹)	R^2	k_1 (min ⁻¹)	R^2	k_2 (g/mg.min)	R^2
Initial OG Concentration (mg/L)	25	94.4	97	0.066	0.447	0.076	0.668	0.166	0.941
	35	93	93.8	0.15	0.526	0.075	0.792	0.066	0.986
	50	90.2	92.5	0.233	0.566	0.067	0.803	0.028	0.977
	65	82	85	0.291	0.717	0.054	0.877	0.0122	0.978
	75	75.5	76.3	0.327	0.738	0.044	0.872	0.007	0.952
	Average R^2				0.599		0.802		0.967
Initial H ₂ O ₂ Concentration (mmol/L)	1.7	50.9	53.5	0.134	0.52	0.017	0.576	0.002	0.641
	2.64	61.7	76.7	0.148	0.561	0.025	0.655	0.004	0.762
	3.52	85.1	86.5	0.236	0.754	0.059	0.935	0.019	0.933
	4.4	71	77.6	0.19	0.602	0.034	0.728	0.007	0.851
	5.28	69.9	75.8	0.193	0.63	0.033	0.768	0.007	0.875
	Average R^2				0.613		0.732		0.812
G-Fe/Cu-NPs Doses (g/L)	0.4	85.1	86.5	0.236	0.754	0.059	0.935	0.019	0.933
	0.7	84.2	87.6	0.228	0.718	0.054	0.921	0.016	0.976
	1.0	89.8	91.6	0.234	0.67	0.068	0.921	0.012	0.975
	1.3	80.7	83.8	0.258	0.72	0.048	0.906	0.011	0.982
	1.6	63.5	69.3	0.17	0.88	0.03	0.952	0.006	0.962
	Average R^2				0.748		0.927		0.966
Initial pH	2	73.4	76.1	0.17	0.521	0.034	0.639	0.008	0.784
	3	90.2	92.5	0.233	0.566	0.067	0.803	0.028	0.978
	4	89.8	91.6	0.234	0.671	0.068	0.921	0.028	0.975
	5	14.6	17.3	0.042	0.851	0.005	0.867	0.0005	0.881
	7	7.3	9.3	0.024	0.945	0.002	0.95	0.096	0.951
	Average R^2				0.711		0.836		0.914
Temperature (°C)	20	86.5	87.3	0.252	0.739	0.061	0.943	0.019	0.979
	30	90.2	92.5	0.233	0.566	0.067	0.803	0.028	0.977
	40	94.8	95.3	0.243	0.543	0.087	0.854	0.058	0.995
	50	94.7	90.3	0.22	0.47	0.078	0.718	0.052	0.964
Average R^2				0.579		0.829		0.979	
NaCl (g/L)	0	94.8	95.3	0.243	0.543	0.087	0.854	0.058	0.995
	0.1	90.2	92.5	0.235	0.577	0.069	0.773	0.03	0.865
	10	94.8	95.3	0.208	0.636	0.054	0.828	0.018	0.95
	50	94.7	90.3	0.182	0.674	0.033	0.804	0.006	0.916
Average R^2				0.607		0.814		0.931	

Thermodynamic of OG Degradation by Fenton-like Reactions

The degradation of OG via heterogeneous Fenton-like reaction catalyzed by G-Fe/Cu-NPs was investigated at various temperatures (293, 303, 313, and 323 K) to determine the reaction spontaneity and the nature of the reaction. These properties of the OG degradation process can be found from the thermodynamic parameters of standard Gibbs free energy (ΔG°), standard enthalpy (ΔH°), and standard entropy (ΔS°) that calculated by Eyring equation³⁴:

$$\ln\left(\frac{k}{T}\right) = \left[\ln\left(\frac{k_B}{h}\right) + \left(\frac{\Delta S^\circ}{R}\right) \right] - \frac{\Delta H^\circ}{R} \cdot \frac{1}{T} \quad \dots 11$$

Where k is the rate controls the reaction⁵¹, T is the absolute temperature (K), k_B is the constant of Boltzman (1.3806×10^{-23} J/K), R is a general constant for gases (8.314 J/mol.K), and h is the Plank's constant (6.6026×10^{-34} J.s).

Hence, ΔS° and ΔH° can be obtained through the intercept and slope of graph $\ln(k/T)$ versus $1/T$ of Eyring equation as depicted in Fig. 15a, thereby ΔG° would be found from the below equation:

$$\Delta G^\circ = \Delta H^\circ - T \Delta S^\circ \quad \dots 12$$

Furthermore, the activation energy can be obtained from the Arrhenius equation shown below

$$\ln k = \ln A - \frac{E_a}{RT} \quad \dots 13$$

Where E_a is the activation energy (kJ/mol), and A is the Arrhenius constant (J/mol.K). E_a

represents the slope of plot between $\ln k$ versus $1/T$ as shown in Fig. 15b.

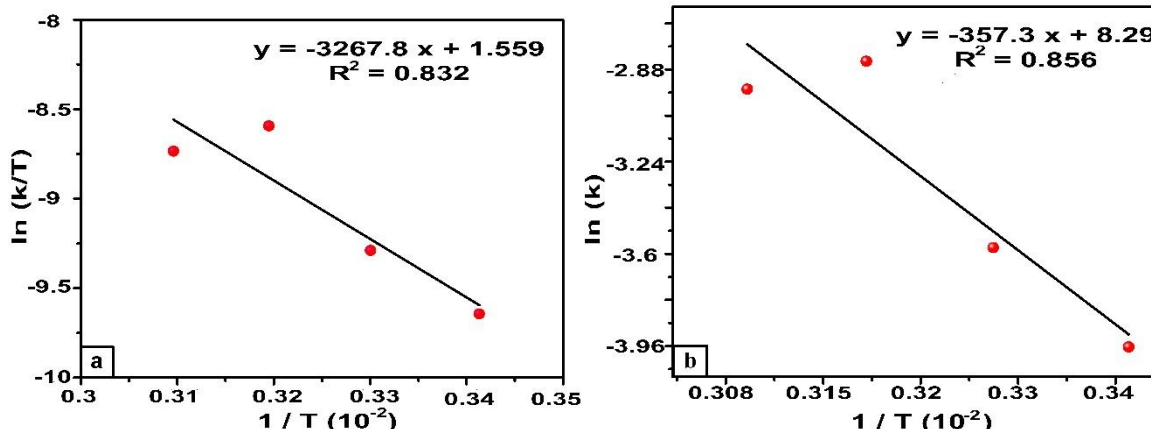


Figure 15. Thermodynamic parameters (a) $\ln(k/T)$ against $1/T$ for determination of thermodynamic properties, and (b) $\ln k$ against $1/T$ to estimate E_a at initial concentration of 50 mg/L, $H_2O_2=3.52$ mmol/L, pH=3, and 300 rpm with a catalyst dose of 1.0 g/L.

In the current case, the rate constant of second-order (k_2) is the rate controls of the reaction. Therefore, the thermodynamic parameters of OG degradation are illustrated in Table 5.

Table 5. Thermodynamic parameters for the removal of OG.

Parameter	Value
ΔG° (kJ/mol)	84.03
ΔH° (kJ/mol)	27.168
ΔS° (J/mol.K)	-185
E_a (kJ/mol)	29.725
A	3.97×10^3

The results for different studied temperatures illustrate that the Gibbs free energy ΔG° had a positive value and lied in the range 81.259 - 86.8 kJ/mol (the average was 84.03 kJ/mol), thus confirms the nonspontaneous reaction nature, on the other hand, the positive value obtained for ΔH° (27.168 kJ/mol) indicated that process of degradation OG via Fenton-like was an endothermic process, in addition, the value of (ΔS°) was negative (-184.6 J/mol.K) which indicated the endergonic process. This result is consistent with the previous study of pretreated pulping effluent by the Fenton-like process reported by ⁵². Moreover, the Fenton-like reaction needed not high energy barrier as revealed from the value of E_a (29.725 kJ/mol) this value of energy agreed with the research article studied by ³⁴.

Conclusion:

In this work, Iron/copper nanoparticles are prepared by green synthesis using the extracts of ficus leaves and applied for the processing of orange G dye from wastewater. The good stable,

amorphous, rounded and shaped as spherical of G-Fe/Cu-NPs are found with the size ranged 32-59 nm and the surface area was 4.452 m²/g. The maximum degradation efficiency of OG is 94.8% in the first 30 min and reaches 95.3% at the final 120 min contact time. It is found that the best value of the heterogeneous Fenton parameters such as hydrogen peroxide concentration, G-Fe/Cu-NPs dose, pH, initial OG concentration, and the temperature is 3.52 mmol/L, 1 g/L, 7, 50 mg/L, and 40 °C respectively. The kinetic study exhibits that the degradation of OG by Fenton-like reactions catalyzed by G-Fe/Cu-NPs fit the second-order kinetic model. Also, the reaction thermodynamic parameters clarify the non-spontaneity nature, endothermic process, and endergonic process. Finally, the value of activation energy (29.725 kJ/mol) illustrates that the Fenton-like reaction need not be as a high energy barrier.

Authors' declaration:

- Conflicts of Interest: None.
- We hereby confirm that all the Figures and Tables in the manuscript are mine ours. Besides, the Figures and images, which are not mine ours, have been given the permission for republication attached with the manuscript.
- Ethical Clearance: The project was approved by the local ethical committee in Ministry of Science and Technology.

Authors' contributions statement:

A.K. H. has designed the experiments and corrected the manuscript, M. A. A. has supervised the work, critically revised the manuscript, and proved the manuscript, and I. M. L. has collected

the data, analyzed/interpreted the results, and drafted the manuscript.

References:

1. Rosly NZ, Abdullah AH, Ahmad Kamarudin M, Ashari SE, Alang Ahmad SA. Adsorption of Methylene Blue Dye by Calix[6]Arene-Modified Lead Sulphide (Pbs): Optimisation Using Response Surface Methodology. *Int J Environ Res Public Health*. 2021; 18(2), 379. [doi:10.3390/ijerph18020397](https://doi.org/10.3390/ijerph18020397).
2. Cai Z, Sun Y, Liu W, Pan F, Sun P, Fu J. An overview of nanomaterials applied for removing dyes from wastewater. *Environ Sci Pollut Res*. 2017; 24(19): 15882–15904.
3. Gičević A, Hindija L, Karačić A. Toxicity of azo dyes in pharmaceutical industry. Springer International Publishing: IFMBE Proc. 2020; 73(1): 581–587.
4. Imam SS, Muhammad AI, Babamale HF, Zango ZU. Removal of Orange G Dye from Aqueous Solution by Adsorption: A Short Review. *J Environ Treat Tech*. 2021; 9(1): 318–327.
5. Katheresan V, Kansedo J, Lau SY. Efficiency of various recent wastewater dye removal methods: A review. *J Environ Chem Eng*. 2018; 6(4):4676–4697.
6. Atiya MA, M-Ridha MJ, Saheb MA. Removal of aniline blue from textile wastewater using electrocoagulation with the application of the response surface approach. *Iraqi J. Sci*. 2020; 61(11): 2797–2811.
7. Önal ES, Yatkin T, Ergüt M, Özer A. Green Synthesis of Iron Nanoparticles by Aqueous Extract of *Eriobotrya japonica* Leaves as a Heterogeneous Fenton-like Catalyst: Degradation of Basic Red 46. *Int. J Chem Eng Appl*. 2017; 8(5): 327–333.
8. Hassan AK, Al-Kindi GY, Ghanim D. Green synthesis of bentonite-supported iron nanoparticles as a heterogeneous Fenton-like catalyst: Kinetics of decolorization of reactive blue 238 dye. *Water Sci Eng*. 2020; 13(4): 286–298.
9. AL-Saade K, Al- Saidi S, Juad H. Degradation of Brilliant Green by Using a bentonite Clay- Based Fe Nano Composite Film as a Heterogeneous Photo-Fenton Catalyst. *Baghdad Sci J*. 2016; 13(3): 524–530.
10. Wang D, Zou J, Cai H, Huang Y, Li F, Cheng Q. Effective degradation of Orange G and Rhodamine B by alkali-activated hydrogen peroxide: roles of HO₂⁻ and O₂⁻. *Environ. Sci. Pollut. Res*. 2019; 26(2): 1445–1454.
11. Li R, Gao Y, Jin X, Chen Z, Megharaj M, Naidu R. Fenton-like oxidation of 2,4-DCP in aqueous solution using iron-based nanoparticles as the heterogeneous catalyst. *J Colloid Interface Sci*. 2015; 438(1): 87–93.
12. Pasinszki T, Krebsz M. Synthesis and application of zero-valent iron nanoparticles in water treatment, environmental remediation, catalysis, and their biological effects. *Nanomaterials*. 2020; 10(5): 917 [doi:10.3390/nano10050917](https://doi.org/10.3390/nano10050917).
13. Ma P, Liu Q, Liu P, Li H, Han X, Liu L *et al*. Green synthesis of Fe/Cu oxides composite particles stabilized by pine needle extract and investigation of their adsorption activity for norfloxacin and ofloxacin. *J Dispers Sci Technol* 2021; 42(9): 1350–1367
14. Alwash A. The green synthesise of zinc oxide catalyst using pomegranate peels extract for the photocatalytic degradation of methylene blue dye. *Baghdad Sci. J*. 2020; 17(3): 787–794.
15. Abd El-Aziz HM, Farag RS, Abdel-Gawad SA. Removal of contaminant metformin from water by using *Ficus benjamina* zero-valent iron/copper nanoparticles. *Nanotechnol Environ Eng* 2020; 5(3): 1–9.
16. Al-Qahtani KM. Cadmium removal from aqueous solution by green synthesis zero valent silver nanoparticles with *Benjamina* leaves extract. *Egypt J Aquat Res* 2017; 43(4): 269–274.
17. Puthukkara P AR, Jose T S, S D lal. Plant mediated synthesis of zero valent iron nanoparticles and its application in water treatment. *J Environ Chem Eng*. 2021; 9(1): (1-77) [doi:10.1016/j.jece.2020.104569](https://doi.org/10.1016/j.jece.2020.104569).
18. Fu F, Dionysiou DD, Liu H. The use of zero-valent iron for groundwater remediation and wastewater treatment: A review. *J Hazard. Mater*. 2014; 267(4): 194–205.
19. Gopal G, Sankar H, Natarajan C, Mukherjee A. Tetracycline removal using green synthesized bimetallic nZVI-Cu and bentonite supported green nZVI-Cu nanocomposite: A comparative study. *J. Environ. Manage*. 2020; 254(2): 109812 [doi:10.1016/j.jenvman.2019.109812](https://doi.org/10.1016/j.jenvman.2019.109812).
20. Dhruval SR, Pai N, Dhanwant SS, Hussein B, Nayak S, Rao CV *et al*. Rapid synthesis of antimicrobial Fe/Cu alloy nanoparticles using Waste Silkworm Cocoon extract for cement mortar applications. *Adv Nat Sci Nanosci Nanotechnol*. 2020; 11(2): 025006 [doi:10.1088/2043-6254/ab8790](https://doi.org/10.1088/2043-6254/ab8790).
21. Galdames A, Ruiz-Rubio L, Orueta M, Sánchez-Arzalluz M, Vilas-Vilela JL. Zero-valent iron nanoparticles for soil and groundwater remediation. *Int J Environ Res Public Health* 2020; 17(16): 1–23.
22. Abdel-Aziz HM, Farag RS, Abdel-Gawad SA. Removal of caffeine from aqueous solution by green approach using *Ficus Benjamina* zero-valent iron/copper nanoparticles. *Adsorpt Sci Technol*. 2020; 38(9-10): 325–343.
23. Abdel-Aziz HM, Farag RS, Abdel-Gawad SA. Carbamazepine Removal from Aqueous Solution by Green Synthesis Zero-Valent Iron/Cu Nanoparticles with *Ficus Benjamina* Leaves' Extract. *Int J Environ Res*. 2019; 13(5): 843–852.
24. Wang J, Liu C, Li J, Luo R, Hu X, Sun X *et al*. In-situ incorporation of iron-copper bimetallic particles in electrospun carbon nanofibers as an efficient Fenton catalyst. *Appl. Catal. B Environ*. 2017; 207(8): 316–325.
25. Suvarna AR, Shetty A, Anchan S, Kabeer N, Nayak S. *Cyclea peltata* Leaf Mediated Green Synthesized Bimetallic Nanoparticles Exhibits Methyl Green Dye Degradation Capability. *Bionanoscience*. 2020; 10(3):

- 606–617.
26. Mohamed EA. Green synthesis of copper & copper oxide nanoparticles using the extract of seedless dates. *Heliyon*. 2020; 6(1): e03123. doi:10.1016/j.heliyon.2019.e03123.
27. Elahimehr Z, Nemati F, Elhampour A. Synthesis of a magnetic-based yolk-shell nano-reactor: A new class of monofunctional catalyst by Cu0-nanoparticles and its application as a highly effective and green catalyst for A3 coupling reaction. *Arab J Chem*. 2020; 13(1): 3372–3382.
28. Khashij M, Dalvand A, Mehralian M, Ebrahimi AA, Khosravi R. Removal of reactive black 5 dye using zero valent iron nanoparticles produced by a novel green synthesis method. *Pigment Resin Technol*. 2020; 49(3): 215–221.
29. Nasrollahzadeh M, Sajadi SM, Khalaj M. Green synthesis of copper nanoparticles using aqueous extract of the leaves of *Euphorbia esula* L and their catalytic activity for ligand-free Ullmann-coupling reaction and reduction of 4-nitrophenol. *Rsc Adv*. 2014; 4(88): 47313–47318.
30. Shaker Ardakani L, Alimardani V, Tamaddon AM, Amani AM, Taghizadeh S. Green synthesis of iron-based nanoparticles using *Chlorophytum comosum* leaf extract: methyl orange dye degradation and antimicrobial properties. *Heliyon*. 2021; 7(2): e06159. doi:10.1016/j.heliyon.2021.e06159.
31. Wang X, Jiang C, Hou B, Wang Y, Hao C, Wu J. Carbon composite lignin-based adsorbents for the adsorption of dyes. *Chemosphere*. 2018; 206(17): 587–596.
32. Kuang Y, Wang Q, Chen Z, Megharaj M, Naidu R. Heterogeneous Fenton-like oxidation of monochlorobenzene using green synthesis of iron nanoparticles. *J Colloid Interface Sci*. 2013; 410(22): 67–73.
33. Kakavandi B, Takdastan A, Pourfadakari S, Ahmadmoazzam M, Jorfi S. Heterogeneous catalytic degradation of organic compounds using nanoscale zero-valent iron supported on kaolinite: Mechanism, kinetic and feasibility studies. *J Taiwan Inst Chem Eng*. 2019; 96(3): 329–340.
34. Giwa ARA, Bello IA, Olabintan AB, Bello OS, Saleh TA. Kinetic and thermodynamic studies of fenton oxidative decolorization of methylene blue. *Heliyon*. 2020; 6(8): e04454. doi:10.1016/j.heliyon.2020.e04454
35. N, Benamor A, Nasser MS, Ba-Abbad MM, El-Naas MH, Mohammad AW. Effective Heterogeneous Fenton-Like degradation of Malachite Green Dye Using the Core-Shell Fe3O4@SiO2 Nano-Catalyst. *ChemistrySelect*. 2021; 6(4): 865–875.
36. Sukla Baidya K, Kumar U. Adsorption of brilliant green dye from aqueous solution onto chemically modified areca nut husk. *South African J Chem Eng*. 2021; 35(1): 33–43.
37. Nadeem N, Zahid M, Tabasum A, Mansha A, Jilani A, Bhatti IA *et al*. Degradation of reactive dye using heterogeneous photo-Fenton catalysts: ZnFe2O4 and GO-ZnFe2O4 composite. *Mater Res Express*. 2020; 7(1): 015519 doi:10.1088/2053-1591/ab66ee.
38. Park JH, Wang JJ, Xiao R, Tafti N, DeLaune RD, Seo DC. Degradation of Orange G by Fenton-like reaction with Fe-impregnated biochar catalyst. *Bioresour Technol* 2018; 249(3): 368–376.
39. Xavier S, Gandhimathi R, Nidheesh PV, Ramesh ST. Comparison of homogeneous and heterogeneous Fenton processes for the removal of reactive dye Magenta MB from aqueous solution. *Desalin Water Treat*. 2015; 53(1): 109–118.
40. Bao C, Zhang H, Zhou L, Shao Y, Ma J, Wu Q. Preparation of copper doped magnetic porous carbon for removal of methylene blue by a heterogeneous Fenton-like reaction. *Rsc Adv*. 2015; 5(88): 72423–72432.
41. Ergüt M, Özer A. Heterogeneous Fenton-like decolorization of Procion Red MX-5B with iron-alginate gel beads as an effective catalyst. *The Glas*. 2019; 13(4): 297–304.
42. Ahmad ARD, Imam SS, Oh W Da, Adnan R. Fe3O4-zeolite hybrid material as hetero-fenton catalyst for enhanced degradation of aqueous ofloxacin solution. *Catalysts*. 2020; 10(11): 1–19.
43. Hassan AK, Rahman MM, Chattopadhyay G, Naidu R. Kinetic of the degradation of sulfanilic acid azochromotrop (SPADNS) by Fenton process coupled with ultrasonic irradiation or L-cysteine acceleration. *Environ Technol Innov*. 2019; 15(3): 100380 doi:10.1016/j.eti.2019.100380.
44. Hashemian S. Fenton-like oxidation of malachite green solutions: Kinetic and thermodynamic study. *J Chem*. 2013; 2013(4): 1-7 doi:10.1155/2013/809318.
45. Hussain S, Aneggi E, Goi D. Catalytic activity of metals in heterogeneous Fenton-like oxidation of wastewater contaminants: a review. *Environ. Chem. Lett*. 2021; 19(3): 2405–2424.
46. Durgut M, Kaya Ş, AŞÇI Y. Using Iron-Containing Metal Oxide as Catalyst for Heterogeneous Fenton Process in Textile Industry Wastewater. *J ESOGU Engin Arch Fac*. 2021, 29(1), 110-117.
47. Liang X, Zhong Y, He H, Yuan P, Zhu J, Zhu S *et al*. The application of chromium substituted magnetite as heterogeneous Fenton catalyst for the degradation of aqueous cationic and anionic dyes. *Chem Eng J*. 2012; 191(10): 177–184.
48. Emami F, Tehrani-Bagha AR, Gharanjig K, Menger FM. Kinetic study of the factors controlling Fenton-promoted destruction of a non-biodegradable dye. *Desalination*. 2010; 257(1-3): 124–128.
49. Santana CS, Ramos MDN, Velloso CCV, Aguiar A. Kinetic evaluation of dye decolorization by fenton processes in the presence of 3-hydroxyanthranilic acid. *Int. J. Environ. Res. Public Health*. 2019; 16(9): 1602 doi:10.3390/ijerph16091602.
50. Youssef NA, Shaban SA, Ibrahim FA, Mahmoud AS. Degradation of methyl orange using Fenton catalytic reaction. *Egypt J Pet*. 2016; 25(3): 317–321.
51. El Haddad ME, Regti A, Laamari MR, Mamouni R, Saffaj N. Use of fenton reagent as advanced oxidative process for removing textile dyes from aqueous solutions. *J Mater Environ Sci*. 2014; 5(3): 667–674.
52. Lal K, Garg A. Utilization of dissolved iron as

catalyst during Fenton-like oxidation of pretreated pulping effluent. Process Saf Environ Prot. 2017; 111(7): 766-774.

التخليق الأخضر للجسيمات النانوية حديد/نحاس كمحفزات في التفاعلات الشبيهة بالفنتون لغرض إزالة الصبغة البرتقالية G

عماد ماجد لعبيي²

محمد عبد عطيه²

أحمد خضير حسان¹

¹مركز بحوث البيئة والمياه، وزارة العلوم والتكنولوجيا، بغداد، العراق
²كلية الهندسة الخوارزمي، جامعة بغداد، بغداد، العراق

الخلاصة:

تدرس هذه الورقة البحثية استخدام طريقة صديقة للبيئة وغير مكلفة لإزالة الصبغة البرتقالية G (OG) من المحلول المائي، حيث تم استخدام مستخلص أوراق شجرة الفيكس لغرض التخليق الأخضر لجسيمات الحديد/نحاس ثنائية الفلز النانوية (G-Fe/Cu-NPs). بعد أن تم تحضير G-Fe/Cu-NPs تم تشخيصها باستخدام مجهر المساح الإلكتروني، BET، مجهر القوة الذرية، مطياف الطاقة المشتتة، مطيافية الأشعة تحت الحمراء، وقياس زيتا. أظهرت نتائج التشخيص بأن شكل G-Fe/Cu-NPs كان مستدير شبه كروي ويتراوح الحجم بين 32-59 نانومتر بينما كانت مساحتها السطحية 4.452 م²/غم. فيما بعد استخدمت الجسيمات النانوية الناتجة كعامل مساعد في تفاعلات الأكسدة الشبيهة بالفنتون. حيث أن كفاءة تحلل صبغة OG اعتمدت بشكل كبير على تركيز الهيدروجين بيروكساييد (1.7-5.28 ملي مولاري)، كمية العامل المساعد (0.4-1.6 غم/لتر)، درجة الحمضية (2-7)، تركيز OG الابتدائي (25-75 ملغم/لتر) ودرجة الحرارة (20-50 درجة مئوية). أظهرت التجارب الدفعية أن 94.8% لتركيز 50 ملغم/لتر من صبغة OG تمت إزالته عند الظروف المثلى للهيدروجين بيروكساييد، كمية العامل المساعد، درجة الحمضية، ودرجة الحرارة والتي كانت 3.52 ملي مولاري، 1 غم/لتر، 3، و 40 درجة مئوية على التوالي خلال زمن مقداره 30 دقيقة. أيضاً أظهرت نتائج دراسة النماذج الحركية بأن إزالة صبغة OG تتبع نموذج حركي من الدرجة الثانية. أخيراً، تم دراسة الديناميكية الحرارية للتفاعل وحُصنت إلى ان التفاعل ماصاً للحرارة وله طاقة تنشيط مقدارها 29.725 كيلوجول/مول.

الكلمات الافتتاحية: شبيهة بالفنتون، التخليق الأخضر، جسيمات الحديد/نحاس النانوية، الحركية، الصبغة البرتقالية G.